

Squeezed States Generation using Cryogenic InP HEMT Transistor Nonlinearity

Ahmad Salmanoglu

Cankaya University, Engineering faculty, Electrical and Electronic Department, Ankara, Turkey

Abstract: This study focuses on generating and manipulating squeezed states with two external oscillators coupled by an InP HEMT transistor operating at cryogenic temperatures. First, the small-signal nonlinear model of the transistor at high frequency at 5 K is analyzed using quantum theory, and the related Lagrangian is theoretically derived. Subsequently, the total quantum Hamiltonian of the system is derived using Legendre transformation. The Hamiltonian of the system includes linear and nonlinear terms, by which the effects on the time evolution of the states are studied. The main result shows that the squeezed state can be generated owing to the nonlinearity of the transistor, and more importantly, it can be manipulated by some specific terms introduced in the nonlinear Hamiltonian. In fact, the nonlinearity of the transistors induces some effects such as capacitance, inductance, and second-order transconductance, by which the properties of the external oscillators are changed. These changes may lead to squeezing or manipulation of the parameters related to squeezing in the oscillators. In addition, it is theoretically derived that the circuit can generate two-mode squeezing. Finally, second-order correlation (photon counting statistics) is studied as a complementary task, and the results demonstrate that the designed circuit exhibits antibunching, where the quadrature operator shows squeezing behavior.

Introduction

The squeezing state and its applications have been developed in recent decades [1-3]. It has been shown that squeezing originates from nonlinearity effects in any systems [1-7]. Different approaches and systems have been employed to generate squeezed state [3-5]. For instance, phase conjugate mirrors using four-wave mixing interactions have been applied to create a squeezed state [1,8]. Another important option is the use of a parametric amplifier, in which three-wave mixing is used to generate the squeezed state [5,7]. In addition, by controlling the spontaneous emission, a two-photon laser is applied to produce a squeezed state [1]. Moreover, atomic interaction with an optical wave can produce a nonlinear medium, leading to the creation of a squeezed state. Additionally, other phenomena such as third-order nonlinearity of the wave propagation in the optical fiber have the ability to generate a squeezed state [7]. In quantum applications, the squeezed state is very important because it introduces less fluctuation in one quadrature phase than the coherent state, which is very similar to the classical state [9-13]. Quantum fluctuation in a coherent state is equal to zero-point fluctuation, in which the standard quantum limits the reduction of the noise in a signal [1, 14]. Therefore, the noise fluctuation can be reduced below the standard limit when the

system is in squeezed state [14]. There is no classical analog for the squeezed state, and this state, in contrast to the coherent state that shows Poisson photon counting (photon bunching) statistics, may show sub-Poisson photon counting (photon antibunching) [1,2, 13-14]. In other words, there is no direct connection between squeezing and photon antibunching, but each is a nonclassical phenomenon [1,3, 13]. For some quantum applications, such as quantum radar and quantum sensors [15-21] the noise effect is critical when the system tries to detect a very low-level signal. For signal detection, the received signals, which have very small levels, can be easily affected by noise. Therefore, to control and limit the noise, it is necessary to prepare the key subsystems, such as the low-noise amplifier (LNA) and detector, to operate in the squeezed state by which the noise can be reduced below the zero-point fluctuation. LNA is an electronic amplifier generally designed to amplify low-level signals while simultaneously keeping the noise at a very low level [23-25]. Today, the cryogenic LNA has been designed to operate at very low temperature to strongly limit the noise and so, due to this fact the cryogenic LNA is so popular in quantum applications [25-30].

With the knowledge of the points mentioned above, in this work, we attempt to design a circuit containing two external oscillators coupled to an InP high electron mobility transistor (HEMT) transistor operating at cryogenic temperature to create the squeezed states. This type of transistor was selected because HEMT technology does not have a strong effect from freeze-out at cryogenic temperature [25-28]. The designed circuit can be considered a core circuit for a low-noise amplifier used in front-end transceivers to amplify faint signals. In this study, the nonlinear properties of the cryogenic InP HEMT transistor play a key role, and we discuss how the emerging nonlinearity can affect the state of the coupling oscillators. Additionally, a critical point will be addressed which relates to the trade-off between squeezing generated by the nonlinear properties of the transistor and the degradation of the produced state because of the damping created by the transistor internal circuits.

Theoretical and Backgrounds

System description

The circuit is schematically shown in Fig. 1, which shows two LC oscillators (resonators) coupled to each other through a nonlinear device (depicted in the inset figure). As mentioned in the previous section, the main goal is to create a squeezing state in a low-noise amplifier (LNA), which is essential in quantum sensing applications [15-16, 26]. In fact, if such a circuit is prepared in the squeezing state, it helps minimize the noise effect. This implies that the performance of the cryogenic LNA, at which the noise strongly limits the operation, is enhanced. Therefore, the circuit shown in Fig.1 is designed. In this circuit, the transistor is used as a nonlinear element, and the state of the oscillators may exhibit-squeezing. It has been theoretically shown that nonlinearity arises because the transistor can be expressed as a nonlinear

capacitor, inductor coupling to the second oscillator, and second-order transconductance (g_{m2-N}). These factors are defined in detail in the next section, and can strongly manipulate the state of the oscillators to create squeezing. Additionally, Fig. 1 schematically reveals that only the second oscillator can generate squeezing in state; this important point will be discussed in detail later. Nonetheless, we theoretically demonstrate that coupling oscillators can generate two-mode squeezing.

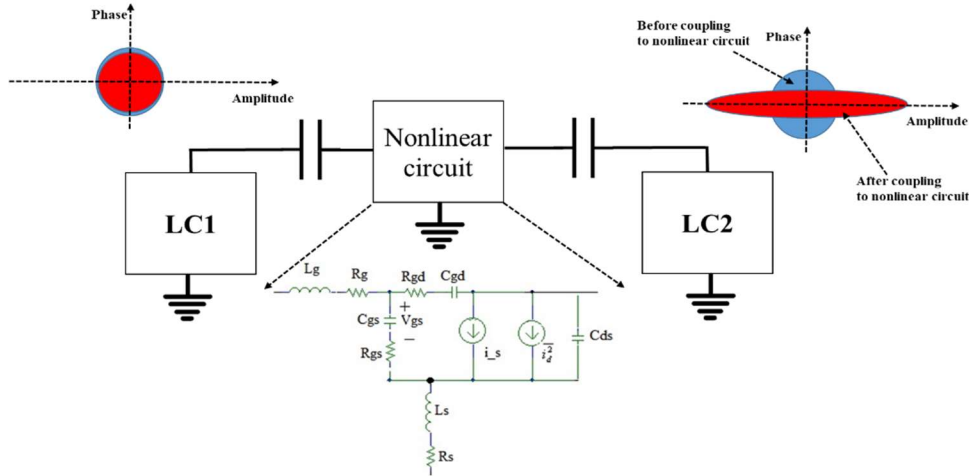


Fig. 1 Schematic of the system containing two external oscillators coupling through a nonlinear device, inset figure: nonlinear device internal circuit

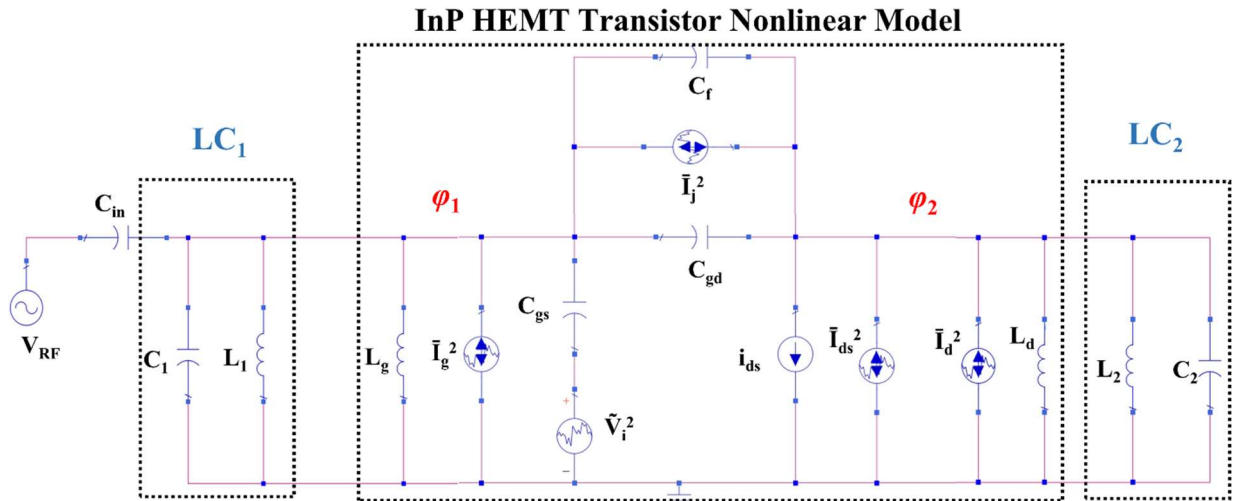


Fig. 2 Complete model of the system; LC1 coupling to LC2 through InP HEMT Transistor operating at 5K.

The high-frequency model of an InP HEMT transistor [26, 28] coupled with two oscillators is shown in Fig. 2. Some elements in the transistor nonlinear model are created owing to the high-frequency effect, such as C_{gs} , C_{gd} , L_g , and L_d and some other elements, such as resistors, as shown in Fig. 1, are created to address the thermal loss in the circuit. These elements are sources of thermal noise in the transistor, and their effects are shown as voltage and current noise sources in Fig. 2. In fact, \bar{I}_g^2 , \bar{I}_j^2 , \bar{I}_d^2 , and \tilde{V}_i^2 models the thermal

noise of R_g , R_{gd} , R_{ds} , and R_{gs} , respectively. A noise model is applied to the circuit to demonstrate the effects of the contributed resistors. Additionally, we ignored the L_s effect and merged R_s with R_{gs} to simplify algebra. In the circuit, i_{ds} and \bar{I}_{ds}^2 are the dependent current sources containing the nonlinearity of the transistor and related thermal noise, which is a critical factor in generating noise. Finally, C_f , C_{in} , V_{RF} , ϕ_1 and ϕ_2 are the feedback capacitor and coupling capacitor used to separate the input signal from the DC signals, input signal, and node flux for the input and output nodes, respectively. This circuit is completely analyzed using quantum theory, and we will attempt to initially derive the contributed Lagrangian; then, the total Hamiltonian of the system is examined, in which the factors that cause the squeezing in state will be addressed.

The designed system Hamiltonian

In this section, the circuit shown in Fig.2 is analyzed using the full quantum theory. As shown in the circuit, it includes all noises that can affect the signals, such as the thermal noises generated by the dependent current source and resistors in the circuit. The data for the nonlinear model of the InP HEMT transistor operating at cryogenic temperatures are listed in Table. 1. First, we theoretically derive the total Lagrangian of the system to obtain the quantum properties of the circuit illustrated in Fig. 2. For the analysis, the coordinate variables are defined as ϕ_1 and ϕ_2 (node flux), as shown in Fig. 2, and the momentum conjugate variables are defined by Q_1 and Q_2 (loop charge). The total Lagrangian of the circuit is derived as [30]:

$$L_c = \frac{C_{in}}{2}(\dot{\phi}_1 - V_{RF})^2 + \frac{C_1}{2}\dot{\phi}_1^2 - \frac{1}{2L_1}\phi_1^2 + \bar{I}_g^2\phi_1 + \frac{C_{gs}}{2}(\phi_1 - \bar{V}_i^2)^2 + \frac{C_{gd} + C_f}{2}(\phi_1 - \phi_2)^2 + i_{ds}\phi_1$$

$$\left(\bar{I}_{ds}^2 + \bar{I}_d^2\right)\phi_2 + \frac{C_2}{2}\dot{\phi}_2^2 - \frac{1}{2L_2}\phi_2^2 + \bar{I}_j^2(\phi_2 - \phi_1)$$
(1)

In this equation the dependent current source is defined as $i_{ds} = g_m V_{gs} + g_{m2} V_{gs}^2 + g_{m3} V_{gs}^3$ [23,31], where g_m is the intrinsic transconductance of the transistor and g_{m2} , g_{m3} are the second- and third-order transconductance. These terms (g_{m2} , g_{m3}) bring nonlinearity in the circuit. Moreover, thermally generated noises by the resistors and the current source are defined as: $\bar{I}_g^2 = 4KT/R_g$, $\bar{I}_d^2 = 4KT/R_d$, $\bar{I}_j^2 = 4KT/R_j$, $\bar{I}_{ds}^2 = 4KT\gamma g_m$, and $\bar{I}_i^2 = 4KT/R_i$, where K , T , and γ respectively are the Boltzmann's constant and operational temperature, and empirical constant [30]. Using the Legendre transformation [14, 30], one can theoretically derive the classical Hamiltonian of the circuit. For this, it is necessary to calculate the momentum conjugate variables using $Q_i = \partial L_c / \partial(\partial\phi_i/\partial t)$ for $i = 1, 2$ represented as:

$$Q_1 = (C_{in} + C_1 + C_{gs} + C_f + C_{gd})\dot{\phi}_1 - (C_f + C_{gd})\dot{\phi}_2 - C_{in}V_{RF} + g_m\phi_2 + 2g_{m2}\phi_2\dot{\phi}_1 + 3g_{m3}\phi_2\dot{\phi}_1^2 - C_{gs}\bar{V}_i^2$$

$$Q_2 = (C_2 + C_f + C_{gd})\dot{\phi}_2 - (C_f + C_{gd})\dot{\phi}_1$$
(2)

Applying Legendre transformation, the classical Hamiltonian is expressed as:

$$H_c = \left\{ \frac{C_A}{2} \dot{\phi}_1^2 + \frac{1}{2L_1} \phi_1^2 + \frac{C_B}{2} \dot{\phi}_2^2 + \frac{1}{2L_2} \phi_2^2 \right\} + \left\{ -C_c \dot{\phi}_1 \dot{\phi}_2 + g_{m2} \phi_2 \dot{\phi}_1^2 + 2g_{m3} \phi_2 \dot{\phi}_1^3 \right\} \quad (3)$$

$$+ \left\{ -\phi_1 (\overline{I_g^2} - \overline{I_j^2}) - \phi_2 (\overline{I_d^2} + \overline{I_j^2} + \overline{I_{ds}^2}) - \frac{C_{gs}}{2} \overline{V_i^2} \right\} - \frac{C_{in}}{2} V_{RF}^2$$

where $C_A = C_{in} + C_1 + C_{gs} + C_f + C_{gd}$, $C_B = C_{gd} + C_f + C_2$, and $C_C = C_f + C_{gd}$. In Eq. 3, the first term relates to the LC resonance Hamiltonian affected by the coupling elements. It is clearly shown that C_A and C_B are affected due to the transistor internal circuit. The second term contributes to the linear and nonlinear coupling between the LC resonators and the nonlinear circuit, and finally the third term defines the noise effect in the system which is originally generated by the transistor nonlinearity in the circuit. In the following, using Eq. 2, one can express the first derivative of the coordinate variables ($\partial\phi_i/\partial t$) in terms of the momentum conjugates (Q_i) represented in the matrix form as:

$$\begin{bmatrix} \dot{\phi}_1 \\ \dot{\phi}_2 \end{bmatrix} = \frac{1}{C_M^2} \left\{ \begin{bmatrix} C_B & C_C \\ C_C & C_A + C_N \end{bmatrix} \begin{bmatrix} Q_1 \\ Q_2 \end{bmatrix} + \begin{bmatrix} C_B & C_C \\ C_C & C_A + C_N \end{bmatrix} \begin{bmatrix} C_{in} & 0 \\ 0 & 0 \end{bmatrix} \begin{bmatrix} V_{RF} \\ 0 \end{bmatrix} - \begin{bmatrix} C_B & C_C \\ C_C & C_A + C_N \end{bmatrix} \begin{bmatrix} 0 & g_m \\ 0 & 0 \end{bmatrix} \begin{bmatrix} \phi_1 \\ \phi_2 \end{bmatrix} \right\} \quad (4)$$

where $C_M^2 = C_B(C_A + C_N) - C_C^2$ and $C_N = 2g_{m2}\phi_{2_dc} + 6g_{m3}\phi_{2_dc}(\partial\phi_1/\partial t)_{dc}$ is the capacitor generated due to the nonlinearity effect. Following, we will show that this quantity strongly affects the coupled LC resonators frequency and impedances and consequently the quantum properties of the LC resonators is severely influenced by C_N . By substitution of Eq. 4 into Eq. 3 one can derive the total Hamiltonian for the system; however, to study in detail about the system and getting to know about each factor's impact in the system, we initially use the linearization technique to linearize the nonlinear terms in the second term of Eq.3 and derive the linear Hamiltonian of the system as: Thus, the linear Hamiltonian of the system is defined as:

$$H_L = \left\{ \frac{1}{2C_{q1}} Q_1^2 + \frac{1}{2L_1} \phi_1^2 + \frac{1}{2C_{q2}} Q_2^2 + \frac{1}{2L_2'} \phi_2^2 \right\} \quad (5)$$

$$\left\{ \frac{1}{2C_{q1q2}} Q_1 Q_2 + g_{12} Q_1 \phi_2 + g_{22} Q_2 \phi_2 \right\} + \left\{ V_{q1} Q_1 + V_{q2} Q_2 + I_{p2} \phi_2 - \overline{I_{gs}^2} \phi_1 \right\}$$

where C_{q1} , C_{q2} , C_{q1q2} , g_{12} , g_{22} , L_2' , V_{q1} , V_{q2} , and I_{p2} are defined in Appendix A and the dc terms are ignored for simplicity. In fact, these coefficients are essentially the function of g_m , C_N , C_C , and V_{RF} by which the nonlinearity effect of the transistor is emphasized. In other words, the nonlinearity created by the transistor induces some factors by which the properties of the coupling LC resonators are strongly affected. For instance, the LC resonators impedances are $Z_1 = \sqrt{L_1}/C_{q1}$, $Z_2 = \sqrt{L_2'}/C_{q2}$, and the associated frequencies are $\omega_1 = 1/\sqrt{L_1 C_{q1}}$, $\omega_2 = 1/\sqrt{L_2' C_{q2}}$. The relations show that the coupling oscillator's impedance and frequencies specially the second LC becomes affected. Additionally, some terms in Eq.2 such as $Q_1 Q_2$, $Q_2 \phi_1$, and $Q_1 \phi_2$ show the coupling between oscillators in the circuit design. Also, in the third term in Eq.5 some terms such as $V_{q1} Q_1$, $\overline{I_{gs}^2} \phi_1$, $V_{g2} Q_2$, $I_{p2} \phi_2$ in the equation declare the RF source and thermal noise coupling to the contributed oscillators. In this equation, $\overline{I_{gs}^2} = \overline{I_g^2} - \overline{I_j^2}$. In the following, one can derive the linear Hamiltonian

in terms of annihilation and creation operators using the quantization procedure for the coordinates and the related momentum conjugates. The quadrature operators defined as $Q_1 = -i(a_1 - a_1^+) \sqrt{(\hbar/2Z_1)}$, $\varphi_1 = (a_1 + a_1^+) \sqrt{(\hbar Z_1/2)}$ and $Q_2 = -i(a_2 - a_2^+) \sqrt{(\hbar/2Z_2)}$, $\varphi_2 = (a_2 + a_2^+) \sqrt{(\hbar Z_2/2)}$, where (a_i, a_i^+) $i = 1, 2$ are the first and second oscillator's annihilation and creation operators. Thus, the linear Hamiltonian in terms of the ladder operators is given by:

$$\begin{aligned}
H_L = & \left\{ \hbar\omega_1 \left(a_1^+ a_1 + \frac{1}{2} \right) + \hbar\omega_2 \left(a_2^+ a_2 + \frac{1}{2} \right) \right\} \\
& + \left\{ -\frac{\hbar}{2} \frac{1}{C_{q1q2} \sqrt{Z_1 Z_2}} (a_1 - a_1^+) (a_2 - a_2^+) - \frac{i\hbar}{2} g_{12} \sqrt{\frac{Z_2}{Z_1}} (a_1 - a_1^+) (a_2 + a_2^+) - \frac{i\hbar}{2} g_{22} (a_2 - a_2^+) (a_2 + a_2^+) \right\} \quad (6) \\
& + \left\{ -iV_{q1} \sqrt{\frac{\hbar}{2Z_1}} (a_1 - a_1^+) - iV_{q2} \sqrt{\frac{\hbar}{2Z_2}} (a_2 - a_2^+) + I_{p2} \sqrt{\frac{\hbar Z_2}{2}} (a_2 + a_2^+) - \overline{I_{gs}^2} \sqrt{\frac{\hbar}{2Z_2}} (a_1 + a_1^+) \right\}
\end{aligned}$$

In the following, it is necessary to add the nonlinearity to the Hamiltonian and derive the total Hamiltonian containing the linear and nonlinear parts. The nonlinear terms in Eq. 3 can be re-written as:

$$H_N = \{g_{m2} + 6g_{m3}\dot{\varphi}_{1_dc}\} \varphi_2 \dot{\varphi}_1^2 \quad (7)$$

Using Eq. 4, the nonlinear Hamiltonian is given by:

$$\begin{aligned}
H_N = g_{m2_N} \left[\left\{ \frac{C_B^2}{C_M^4} \varphi_2 Q^2 + \frac{C_C^2}{C_M^4} \varphi_2 Q^2 + \frac{2C_B C_C}{C_M^4} \varphi_2 Q_2 Q - \frac{2g_m C_B^2}{C_M^4} \varphi_2^2 Q - \frac{2g_m C_B C_C}{C_M^4} \varphi_2^2 Q_2 + \frac{g_m^2 C_B^2}{C_M^4} \varphi_2^3 \right\}_{NL} \right. \\
\left. \left\{ \underbrace{\frac{-2g_m C_B^2 C_{in} V_{RF}}{C_M^4}}_{1/2L_{2N}} \varphi_2^2 + \underbrace{\frac{2C_B^2 C_{in} V_{RF}}{C_M^4}}_{g_{12N}} Q_1 \varphi_2 + \underbrace{\frac{2C_B C_C C_{in} V_{RF}}{C_M^4}}_{g_{22N}} Q_2 \varphi_2 + \underbrace{\frac{C_B^2 V_{in}^2 V_{RF}^2}{C_M^4}}_{I_{p2N}} \varphi_2 \right\}_L \right] \quad (8)
\end{aligned}$$

where $g_{m2_N} = g_{m2} + 6g_{m3} (\partial\varphi_1/\partial t)|_{dc}$. The linear part of the Eq. 8 can directly attach to Eq. 5 to make the modified linear Hamiltonian given by:

$$\begin{aligned}
H_L = & \left\{ \frac{1}{2C_{q1}} Q_1^2 + \frac{1}{2L_1} \varphi_1^2 + \frac{1}{2C_{q2}} Q_2^2 + \left(\frac{1}{2L_2'} + \frac{1}{2L_{2N}} \right) \varphi_2^2 \right\} \\
& \left\{ \frac{1}{2C_{q1q2}} Q_1 Q_2 + (g_{12} + g_{12N}) Q_1 \varphi_2 + (g_{22} + g_{22N}) Q_2 \varphi_2 \right\} + \left\{ V_{q1} Q_1 + V_{q2} Q_2 + (I_{p2} + I_{p2N}) \varphi_2 - \overline{I_{gs}^2} \varphi_1 \right\} \quad (9)
\end{aligned}$$

As clearly seen in Eq. 9, the nonlinear Hamiltonian can change the coupling between oscillators in the circuit and the most important factor is g_{m2_N} by which the coupling between different coordinates and their momentum conjugates are manipulated. Additionally, attachment from Eq. 8 to Eq. 5 leads to change the second resonator's inductance by factor of L_{2N} . The term brought from nonlinearity (L_{2N}) manipulates the second resonator's impedance and frequency. Finally, the nonlinear terms of Eq. 8 are considered and so, the total Hamiltonian of the system in the terms of the ladder operators is given by:

$$\begin{aligned}
H_t = & \left[\left\{ \hbar\omega_1 \left(a_1^+ a_1 + \frac{1}{2} \right) + \hbar\omega_2 \left(a_2^+ a_2 + \frac{1}{2} \right) \right\} \right. \\
& + \left\{ -\frac{\hbar}{2} \frac{1}{C_{q1q2} \sqrt{Z_1 Z_2}} (a_1 - a_1^+) (a_2 - a_2^+) - \frac{i\hbar}{2} g_{12}' \sqrt{\frac{Z_2}{Z_1}} (a_1 - a_1^+) (a_2 + a_2^+) - \frac{i\hbar}{2} g_{22}' (a_2 - a_2^+) (a_2 + a_2^+) \right\} \\
& + \left. \left\{ -iV_{q1} \sqrt{\frac{\hbar}{2Z_1}} (a_1 - a_1^+) - iV_{q2} \sqrt{\frac{\hbar}{2Z_2}} (a_2 - a_2^+) + I_{p2}' \sqrt{\frac{\hbar Z_2}{2}} (a_2 + a_2^+) - \overline{I_{gs}^2} \sqrt{\frac{\hbar}{2Z_2}} (a_1 + a_1^+) \right\} \right]_{\perp L} \quad (10) \\
& + \left[-\hbar g_{13} (a_1 - a_1^+)^2 (a_2 + a_2^+) + \hbar g_{14} (a_2 + a_2^+) (a_2 - a_2^+)^2 - \hbar g_{15} (a_1 - a_1^+) (a_2 - a_2^+) (a_2 + a_2^+) \right. \\
& \left. + \hbar g_{16} (a_2 + a_2^+)^3 + i\hbar g_{17} (a_1 - a_1^+) (a_2 + a_2^+)^2 + i\hbar g_{18} (a_2 - a_2^+) (a_2 + a_2^+)^2 \right]_{NL}
\end{aligned}$$

where $I_{p2}' = I_{p2} + I_{p2N}$, $g_{12}' = g_{12} + g_{12N}$, and $g_{22}' = g_{22} + g_{22N}$. Also, $g_{13} = (1/2Z_1)(\sqrt{\hbar/2Z_2})g_{m2_N}C_B^2/C_M^4$, $g_{14} = (1/2Z_2)(\sqrt{\hbar/2Z_2})g_{m2_N}C_C^2/C_M^4$, $g_{15} = (1/\sqrt{Z_2 Z_1})(\sqrt{\hbar/2Z_2})g_{m2_N}C_B C_C/C_M^4$, $g_{16} = (Z_2/2)(\sqrt{\hbar Z_2/2})g_m^2 g_{m2_N} C_B^2/C_M^4$, $g_{17} = Z_2(\sqrt{\hbar/2Z_1})g_m g_{m2_N} C_B^2/C_M^4$, and $g_{18} = Z_2(\sqrt{\hbar/2Z_2})g_m g_{m2_N} C_B C_C/C_M^4$. It is clearly shown in coefficients from g_{13} to g_{18} in which the effect of g_{m2_N} is dominant. In other words, the nonlinearity of the system in this work is strongly changed and controlled by the second-order transconductance g_{m2_N} . Now, one can show using the total Hamiltonian of the system in which what terms in the presented Hamiltonian in Eq. 10 has the ability to generate the squeezing state.

Generation of the squeezing state

A squeezed-coherent state is generally produced by acting of the squeezed and displacement operators in, on the vacuum state defined mathematically as $|\alpha, \zeta\rangle = D(\alpha)S(\zeta)|0\rangle$, where $|0\rangle$ is the vacuum state [14]. It is found that the coherent state is generated by the linear terms in the Hamiltonian, whereas a squeezed state needs quadratic terms such as a^2 and a^{+2} in the exponent. The squeezed-coherent state $S(\zeta, \alpha)$ can be analyzed as the evolution $\exp[Ht/\hbar]$ under the Hamiltonian defined in Eq. 10. Based on this definition, any quadratic terms such as a^2 and a^{+2} in the Hamiltonian may generate squeezing. The Hamiltonian in Eq. 10, the squeezed state can be generated by:

$$S(\zeta) = \exp \left[\zeta_1 (a_2^2 - a_2^{+2}) + \left(\frac{\zeta_2^*}{2} a_2^2 - \frac{\zeta_2}{2} a_2^{+2} \right) \right] t \quad (11)$$

In this equation the squeezing parameters are defined as $\zeta_1 = -0.5g_{22}' + g_{18}\text{Re}\{A_2\} + jg_{14}\text{Im}\{A_2\}$ and $\zeta_2 = 2A_1^*(-g_{17}-jg_{15})$, where A_1 and A_2 are the strong fields (DC points) of LC_1 and LC_2 . The DC points can be calculated using Heisenberg-Langevin equations in the steady-state [15, 16]. Also $\text{Re}\{\}$ and $\text{Im}\{\}$ indicate the real and imaginary parts, respectively. Eq. 11 clearly shows that the squeezing is generated just for LC_2 and it does not happen for LC_1 . This point contributes to the nonlinearity terms in Hamiltonian expressed in Eq. 10 and also is related to the dependent current source containing g_{m2} and g_{m3} , which is directly connected to LC_2 . The important point about the squeezing strength parameters ζ_1 and ζ_2 is that each

of them is dependent on g_{m2_N} . In Eq. 11, ζ_1 and ζ_2 are complex numbers which means that the squeezing parameters contain the phase which determines the angle of quadrature to be squeezed. Additionally, we found that the system can generate two-mode squeezing. That means that the nonlinearity created by the transistor couples two oscillators in such a way that the coupled modes become squeezed. The expression generated due to the Hamiltonian of the system for two-mode squeezing is expressed as:

$$S_2(\zeta) = \exp \left[\left(\frac{\zeta_{t1}^*}{2} a_1 a_2 - \frac{\zeta_{t1}}{2} a_1^+ a_2^+ \right) + \left(\frac{\zeta_{t2}^*}{2} a_1 a_2 - \frac{\zeta_{t2}}{2} a_1^+ a_2^+ \right) \right] t \quad (12)$$

where $\zeta_{t1} = jA_2 g_{15}$ and $\zeta_{t2} = jA_1 g_{13}$. In the same way, the squeezing parameters are strongly dependent on g_{m2_N} . Finally, one can easily find that the system can generate the coherent state which means that the state generated by the Hamiltonian expressed in Eq. 10 is a squeezed-coherent state or a two-mode squeezed-coherent state. In the following, we just focus on the squeezed-coherent state and study the parameters that can manipulate the squeezing states. For simulation, “ t ” in the exponent ($\exp[Ht/\hbar]$) is defined as $t_0 < \{1/\kappa_1, 1/\kappa_2\}$, where κ_1 and κ_2 are the first and second oscillators decay rate. By selecting t_0 , the system is forced to generate squeezing before the resonator decaying by which the squeezing is destroyed [1]. Some more information is introduced about t_0 in Appendix B.

Table. 1 Values for the small signal model of the 2*50 μm InP HEMT at 5 K [32-34].

	Stands for	Value Unit
R_g	Gate resistance	0.3 Ω
L_g	Gate inductance	75 pH
L_d	Drain inductance	70 pH
C_{gs}	Gate-Source capacitance	69 fF
C_{ds}	Drain-Source capacitance	29 fF
C_{gd}	Gate-Drain capacitance	19 fF
R_{gs}	Gate-Source resistance	4 Ω
R_{gd}	Gate-Drain resistance	35 Ω

In this study, quadrature variance is used to demonstrate the behavior of the state generated by the oscillators. In addition, we used the bunching and antibunching behavior of the generated photons. The second-order correlation function, $g^2(\tau)$, must be calculated. For the designed system, with regard to the fact that the system is limited by t_0 , the photon counting time is sufficiently short. Thus, for such a short counting time, the variance of the photon number distribution is related to the second-order correlation function $g^2(\tau = 0) = 1 + (V(n) - \langle n \rangle) / \langle n \rangle$, where $V(n)$ and $\langle n \rangle$ are the photon number variance and the average, respectively [1, 13]. It has been shown that for light with sub-Poissonian statistics $g^2(\tau = 0) < 1$, this phenomenon is called anti-bunching, which is a nonclassical phenomenon. Of course, $g^2(\tau = 0) < 1$ is not a necessary condition for squeezing the state; however, if $g^2(\tau = 0) > 1$, the field is a classical

field [1]. In other words, the squeezing state may exhibit bunching and antibunching behaviors. In the following section, the aforementioned points are discussed with some related simulations.

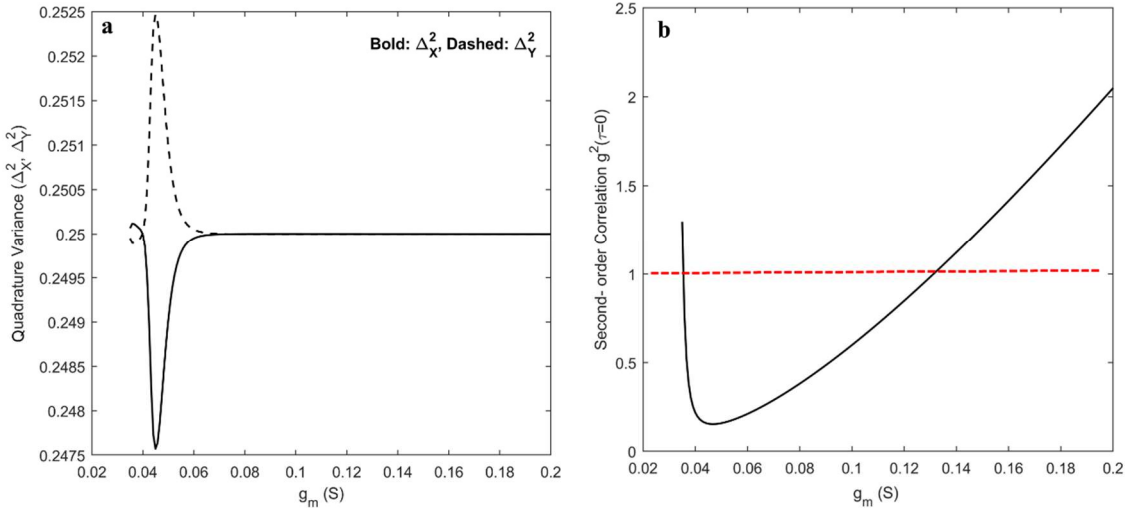


Fig. 3 a) Quadrature variance vs. g_m (S), b) Second-order correlation function vs. g_m (S); $C_f = 0.02$ pF, $g_{m3} = 1200$ mA/V³, $g_{m2} = 200$ mA/V², $V_{RF} = 1$ μ V, $\kappa = \kappa_1 = \kappa_2 = 0.001\omega$.

The squeezing of the second oscillator with respect to Eq. 11 is simulated and the results are shown in Fig. 3. As seen in Fig. 3a, which illustrates the quadrature operator's variance versus g_m , the squeezing appears in the resonator and reaches to the maximum value for g_m around 45 mS. However, the amount of the squeezing is decreased when g_m exceeds 60 mS. It may relate to the fact that g_m directly manipulates \bar{I}_{ds}^2 by which the noise exceeds in the system and due to that, the squeezing is strongly limited when g_m is increased. Additionally, in Fig. 3a, the dashed graph shows $\Delta y^2 > 0.25$, indicating that this operator for each value of g_m shows bunching; in other words, the operator shows classical field behavior. We theoretically show that the important factors affecting LC_2 to generate squeezing state include C_N , C_N' , and g_{m2_N} . To get know about the factors effects and make a comparison with other elements, the contributed values are calculated for $g_m = 45$ mS and represented as: $C_N = 3.3$ pF, $C_N' = 72$ mA/V, and $g_{m2_N} = 677$ mA/V². These values show nonlinear effects in the transistor which changes the electrical properties of the circuit. For instance, one can compare C_N with C_{gd} or C_{gs} , which indicates that C_N is greater than the internal capacitances and g_{m2_N} is comparable with g_{m2} .

In addition, the second-order correlation function $g^2(\tau = 0)$ behavior can be considered, as illustrated in Fig. 3b. The figure shows perfect consistency with the quadrature operators' variance around $g_m = 40$ mS. The value of $g^2(\tau = 0)$ around 45 mS reaches its minimum and is less than 1 which means that the second resonator exhibits antibunching. Notably, the change in the sign of $g^2(\tau = 0)$ from bunching ($g^2(\tau = 0) > 1$) to antibunching ($g^2(\tau = 0) < 1$) indicates squeezing in the system. The results shown in Fig. 3b reveal that

squeezing occurs only for small values of g_m . In other words, the current amplification factor (g_m) in the transistor should be maintained at a low level to generate squeezing at cryogenic temperatures. Nonetheless, this is clearly shown in Eq. 11 that ζ_1 and ζ_2 are strongly manipulated by g_{m2-N} which is a fundamental function of g_{m2} , g_{m3} , and that C_N plays a key role in changing the coupling between resonators. Additionally, other factors such as feedback capacitance, LC resonator decay rate, and input RF source can influence the squeezing in the system. For instance, the effect of g_{m3} as a nonlinearity factor on the quadrature operator variance and photon bunching and antibunching is illustrated in Fig. 4. Fig. 4a shows that by increasing g_{m3} the quadrature variance increases. This contributed to the increase in the squeezing strength parameters. In addition, the figure shows that increasing g_{m3} leads to maintaining $\Delta x^2 < 0.25$ for larger g_m . In the same way, the effect of g_{m3} increasing on the second-order correlation function is depicted in Fig. 4b. This reveals that increasing g_{m3} causes an increase in g_m to 120 mS, in which the second-order correlation shows antibunching. This contributes to the fact that increasing g_{m3} changes C_N and g_{m2-N} leading to a strengthening the squeezing behavior.

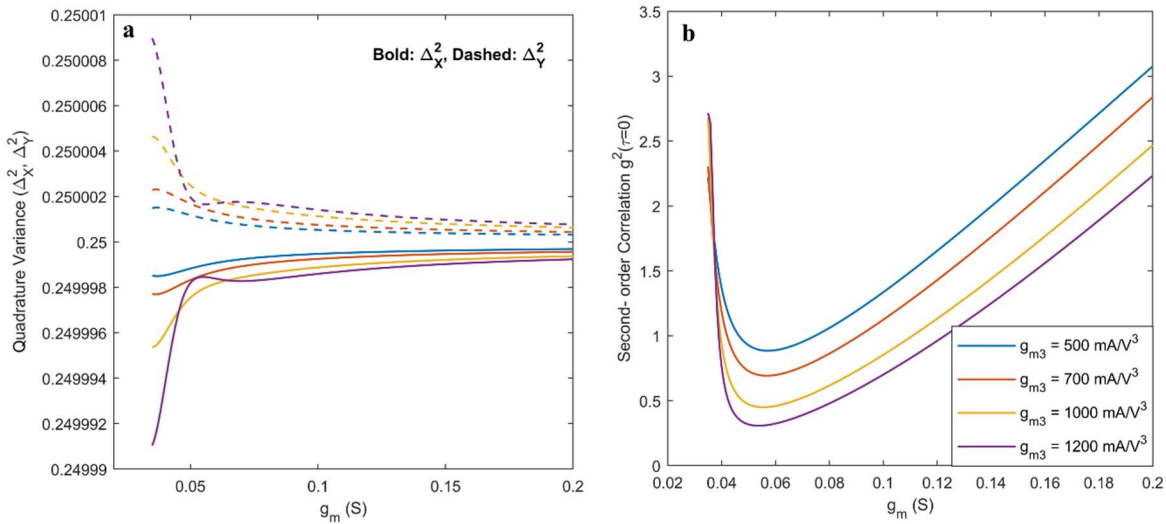


Fig.4 Quadrature variance vs. g_m (S), b) Second-order correlation function vs. g_m (S) for different g_{m3} (mA/V³); $C_f = 0.02$ pF, $g_{m2} = 200$ mA/V², $V_{RF} = 1$ μ V, $\kappa = 0.001\omega$.

Additionally, in this study, the effects of other parameters such as C_f , V_{RF} , g_{m2} , and oscillator decay rate κ are analyzed, and the results of the simulations are depicted in Fig. 5. In this graph, the red dashed line is inserted to easily trace the bunching to antibunching (and vice versa) entry point as a function of g_m . In this simulation, it is assumed that the two oscillators had the same decay rate $\kappa_1 = \kappa_2 = \kappa$. As expected, Fig. 5 shows that increasing C_f , V_{RF} , and g_{m2} causes an increase in antibunching, whereas an increase in the decay rate leads to a decrease in antibunching. In this figure, the key factor that can be freely manipulated it, is the feedback capacitor, by which circuit properties, such as noise, gain, and stability, can be

manipulated. The graph in Fig. 5b reveals that increasing the feedback capacitor causes antibunching for a larger g_m . This may be related to the noise figure enhancement using feedback in the circuit. In other words, using a feedback capacitor strongly enhances the noise figure of the circuit, which means that eliminating noise leads to enhanced squeezing.

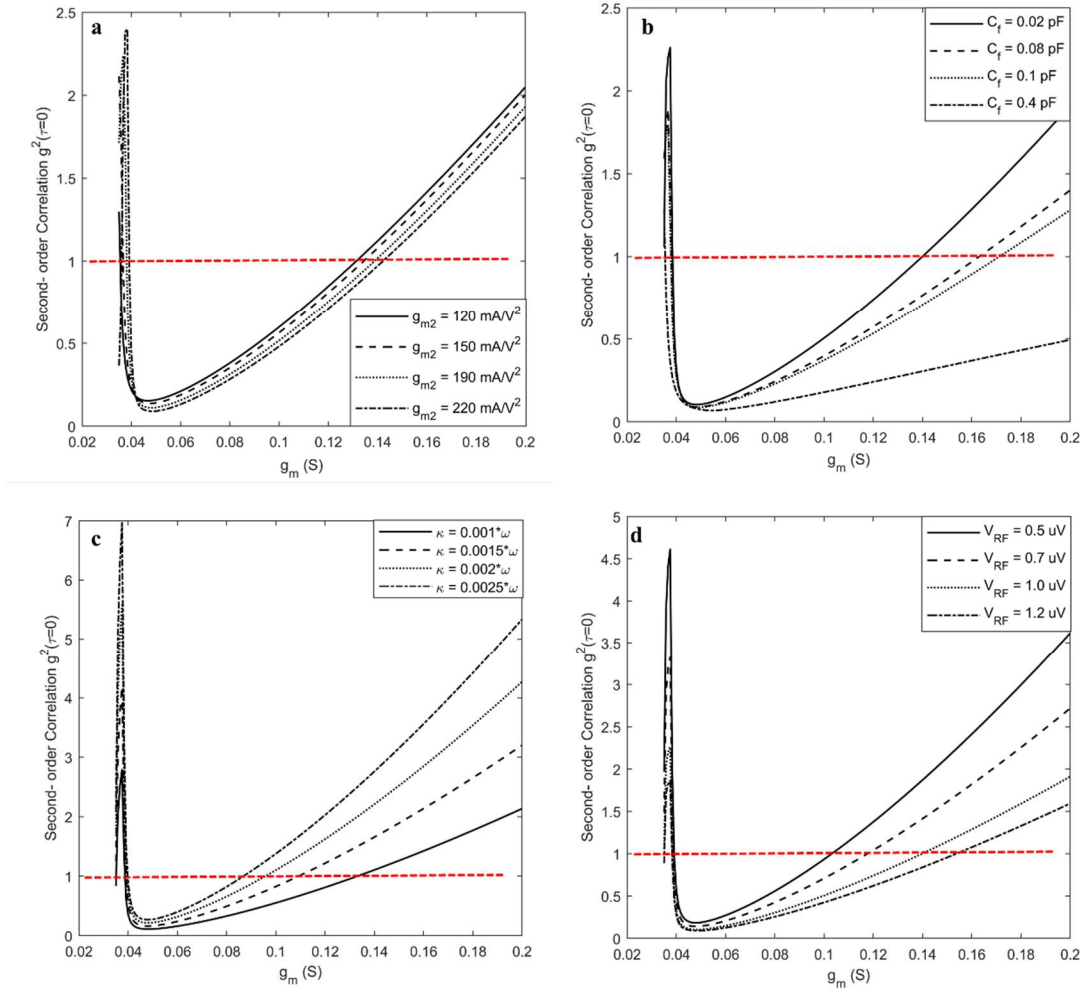


Fig.4 Second-order correlation function vs. g_m (S) a) g_{m2} effect, b) feedback capacitance effect (C_f), c) LC resonator decay rate effect (κ), d) Input RF source amplitude effect (V_{RF}); $g_{m3} = 1200 \text{ mA/V}^3$.

The results illustrated in this study show that cryogenic InP HEMT transistor nonlinearity has the ability to generate a squeezed state. This is an important achievement, because such a system can be an essential part of a cryogenic detector that has been used in quantum applications. Thus, the operation of the detector or amplifier in the squeezed state implies that the noise fluctuation is limited below the zero-point fluctuations. This is an interesting goal of this study; nonetheless, we know that this is challenging to achieve.

Conclusions

This article mainly emphasizes the generation of the squeezing state using the nonlinearity of the InP HEMT transistor. For this purpose, we designed a circuit containing two external oscillators coupled with a cryogenic InP HEMT transistor operating at 5 K. The circuit was analyzed using quantum theory, and the contributions of the Lagrangian and Hamiltonian functions were theoretically derived. Some key factors in the Hamiltonian arise because the nonlinearity of the transistor can generate a squeezed state. Thus, we focused on these parameters and their engineering attempts to generate squeezing. The results show that the squeezed state occurred only for the second oscillator. This implies that the first oscillator experiences a coherent state. In addition, we theoretically demonstrate that two coupled oscillators through a cryogenic transistor have the ability to generate two-mode squeezing. Thus, as a general point, if such a cryogenic circuit has the ability to generate squeezing, then the critical noise fluctuations would be strongly limited. This means that important phenomena, such as entanglement, can persist for a long time in the quantum transceiver.

References

1. D. F. Walls, Squeezed states of light. *Nature* 306, 141–146, 1983. <https://doi.org/10.1038/306141a0>.
2. L. Mandel, Squeezed States and Sub-Poissonian Photon Statistics, *Phys. Rev. Lett.* 49, 136–138, 1982.
3. H. Rodrigues, D. Portes Junior, S. B. Duarte, B. Baseia, squeezing in coupled oscillators having neither nonlinear terms nor time-dependent parameters. *Brazilian Journal of Physics*, 31(4), 562-566, 2001.
4. S. Friberg, L. Mandel, Production of squeezed states by combination of parametric down-conversion and harmonic generation, *Optics Communications*, 48, 439-442, 1984.
5. B. R. Mollow and R. J. Glauber, Quantum Theory of Parametric Amplification. I, *Phys. Rev.* 160, 1076–1096, 1967.
6. M.S. Shahriar, P.R. Hemmer, Generation of squeezed states and twin beams via non-degenerate four-wave mixing in a Λ system, *Optics Communications* 158, 273–286, 1998.
7. A. I. Lvovsky, Squeezed light, arXiv:1401.4118v2 [quant-ph] 28 Jul 2016.
8. Horace P. Yuen and Jeffrey H. Shapiro, Generation and detection of two-photon coherent states in degenerate four-wave mixing, *Optics Letters*. 4, 334-336, 1979.
9. T. Hirano and M. Matsuoka, Broadband squeezing of light by pulse excitation, *Optics Letters*. 15, 1153-1155, 1990.
10. G. Breitenbach, S. Schiller, J. Mlynek, Measurement of the quantum states of squeezed light. *Nature* 387, 471–475, 1997. <https://doi.org/10.1038/387471a0>.

11. Yamamoto Y, Machida S, Richardson WH. Photon number squeezed States in semiconductor lasers. *Science*, 255(5049):1219-24, 1992. doi: 10.1126/science.255.5049.1219. PMID: 17816827.
12. M. T. Raiford, Statistical Dynamics of Quantum Oscillators and Parametric Amplification in a Single Mode, *Phys. Rev. A*, 2, 1541–1557, 1970.
13. Luiz Davidovich, Sub-Poissonian processes in quantum optics, *Reviews of Modern Physics*, Vol. 68, 127-172, 1996.
14. M. O. Scully, M. S. Zubairy, “Quantum Optics”, Cambridge University Press, UK, 1997.
15. A. Salmanoglu, D. Gokcen, Entanglement Sustainability Improvement Using Optoelectronic Converter in Quantum Radar (Interferometric Object-Sensing), *IEEE Sensors Journal* 21, 9054-9062, 2021.
16. A. Salmanoglu, D. Gokcen, H.S. Gecim, Entanglement Sustainability in Quantum Radar, *IEEE J. Sel. Top. Quantum Electron* 26, 1-11, 2020.
17. S. Barzanjeh, S. Pirandola, D. Vitali, and J. M. Fink, “Microwave quantum illumination using a digital receiver”, *Science Advances*, 2020: 6, eabb0451, DOI: 10.1126/sciadv.abb0451.
18. S. Barzanjeh, S. Guha, Ch. Weedbrook, D. Vitali, J. H. Shapiro, and S. Pirandola, “Microwave Quantum Illumination”, *Phys. Rev. Lett.* 114, 080503-8, 2015.
19. A. Salmanoglu, D. Gokcen, Design of quantum sensor to duplicate European Robins navigational system, *Sensors and Actuators A: Physical*, 322, 112636, 2021.
20. A. Salmanoglu, D. Gokcen, and H. S. Gecim, Entanglement of Optical and Microcavity Modes by Means of an Optoelectronic System, *Phys Rev Applied*, 11, 024075-024089, 2019.
21. A. Salmanoglu, H. S. Gecim, Optical and Microcavity Modes Entanglement by Means of Plasmonic Opto-Mechanical System, *IEEE J. Sel. Top. Quantum Electron*, 26, 1016-1030, 2020.
22. V. Aparin and L. E. Larson, Modified Derivative Superposition Method for Linearizing FET Low-Noise Amplifiers, *IEEE Trans. Microw. Theory Techn*, 53, 571-581, 2005.
23. S. Ganesan, E. Sánchez-Sinencio, and J. Silva-Martinez, A Highly Linear Low-Noise Amplifier, *IEEE Trans. Microw. Theory Techn*, 54, 4079-4086, 2006.
24. Z. Hamaizia, N. Sengouga, M. Missous, M.C.E. Yagoub, A 0.4 dB noise figure wideband low-noise amplifier using a novel InGaAs/InAlAs/InP device, *Materials Science in Semiconductor Processing*, 14, 89, 2011.
25. B. Yurke, M. L. Roukes, R. Movshovich, A, N. Pargellis, A low noise series-array Josephson Junction parametric amplifier, *Appl. Phys. Lett.* 69, 3078-3080, 1996, <https://doi.org/10.1063/1.116845>.
26. J. Schlee et al., Ultralow-Power Cryogenic InP HEMT with Minimum Noise Temperature of 1 K at 6 GHz, in *IEEE Electron Device Letters*, 33, 664-666, 2012, doi: 10.1109/LED.2012.2187422.

27. E. Cha, N. Wadefalk, G. Moschetti, A. Pourkabirian, J. Stenarson and J. Grahn, A 300- μ W Cryogenic HEMT LNA for Quantum Computing, 2020 IEEE/MTT-S International Microwave Symposium (IMS), 2020, pp. 1299-1302, doi: 10.1109/IMS30576.2020.9223865.
28. N. Wadefalk, A. Mellberg, I. Angelov, M.E. Barsky, S. Bui, E. Choumas, R.W. Grundbacher, E.L. Kollberg, R. Lai, N. Rorsman, P. Starski, Cryogenic wide-band ultra-low-noise IF amplifiers operating at ultra-low DC power, *IEEE Transactions on Microwave Theory and Techniques*, 51, 1705-1711, 2003.
29. A. Salmanogli, H. S. Gecim, Design of the Ultra-Low Noise Amplifier for Quantum Applications, arXiv preprint arXiv:2111.15358, 2021.
30. A. Salmanogli, Entangled Microwave Photons Generation using Cryogenic Low Noise Amplifier (Transistor Nonlinearity Effects), arXiv preprint arXiv:2201.04893, 2022.
31. X. Fan, H. Zhang, and E. Sánchez-Sinencio, A Noise Reduction and Linearity Improvement Technique for a Differential Cascode LNA, *IEEE J. Solid-State Circuits*, 43, 588, 2008.
32. E. Cha, G. Moschetti, N. Wadefalk, Per-Åke Nilsson; S. Bevilacqua, J. Grqhn, Two-finger InP HEMT design for stable cryogenic operation of ultra-low-noise Ka-band LNAs, *2017 IEEE MTT-S International Microwave Symposium (IMS)*, 168-171, 1979. doi: 10.1109/MWSYM.2017.8058959.
33. E. Cha, N. Wadefalk, G. Moschetti, A. Pourkabirian, J. Stenarson and J. Grahn, InP HEMTs for Sub-mW Cryogenic Low-Noise Amplifiers, in *IEEE Electron Device Letters*, 41, 1005-1008, 2020. doi: 10.1109/LED.2020.3000071.
34. A. Mellberg *et al.*, Cryogenic 2-4 GHz ultralow noise amplifier, *2004 IEEE MTT-S International Microwave Symposium Digest (IEEE Cat. No.04CH37535)*, 161-163 1, 2004. doi: 10.1109/MWSYM.2004.1335830.

Appendixes:

Appendix A:

In this appendix all of the parameters used in the main article listed as C_{q1} [F], C_{q2} [F], C_{q1q2} [F], g_{12} [1/s], g_{22} [1/s], V_{q1} [v], V_{q2} [v] and I_{p2} [A] are given by:

$$\begin{aligned} \frac{1}{C_{q1}} &= \frac{2C_B^2(C_N + 0.5C_A)}{C_M^4} - \frac{C_C^2 C_B}{C_M^4} \\ \frac{1}{C_{q2}} &= \frac{2C_C^2(C_N + 0.5C_A)}{C_M^4} + \frac{C_A'^2 C_B}{C_M^4} - \frac{2C_C(C_N + C_A)C_B}{C_M^4} \\ \frac{1}{C_{q1q2}} &= \frac{2C_C C_B(C_N + 0.5C_A)}{C_M^4} + \frac{C_C(C_N + C_A)C_B}{C_M^4} - \frac{C_C^2 C_B}{C_M^4} \\ \frac{1}{L_{p2}} &= \frac{2g_m^2 C_B^2(C_N + 0.5C_A)}{C_M^4} + \frac{2g_m C_N' C_B}{C_M^2} \\ g_{12} &= \frac{-2g_m C_B^2(C_N + 0.5C_A)}{C_M^4} + \frac{C_N' C_B}{C_M^2} - \frac{3g_m C_C^2 C_B}{2C_M^4} \\ g_{22} &= \frac{-2g_m C_B C_C(C_N + 0.5C_A)}{C_M^4} + \frac{C_N' C_C}{C_M^2} + \frac{g_m C_C^3}{C_M^4} - \frac{g_m(C_N + C_A)C_C C_B}{C_M^4} \\ V_{q1} &= \frac{2C_B C_C C_{in} V_{RF}(C_N + 0.5C_A)}{C_M^4} - \frac{C_C^2 C_{in} C_B V_{RF}}{C_M^4} \\ V_{q2} &= \frac{2C_B C_C C_{in} V_{RF}(C_N + 0.5C_A)}{C_M^4} - \frac{C_C^3 C_{in} V_{RF}}{C_M^4} \\ I_{p2} &= \frac{-2g_m C_B^2 C_{in} V_{RF}(C_N + 0.5C_A)}{C_M^4} + \frac{g_m C_B C_{in} C_C^2 V_{RF}}{C_M^4} - \frac{C_B C_{in} C_N' V_{RF}}{C_M^2} - \overline{I_{ds}^2} \end{aligned}$$

where and $C_N' = 2g_{m2}(\partial\phi_1/\partial t)|_{dc} + 12g_{m3} [(\partial\phi_1/\partial t)|_{dc}]^2$.

Appendix B:

In this appendix, we try to give some information about t_0 . In the main article, it is discussed that t_0 is selected less than the times that two oscillators' decays with it. In fact, from classical point of view, t_0 should be in the order of the steady-state time. Therefore, in this part we tried to calculate the step response of the circuit. For this reason, however for simplicity, a simplified version of the circuit shown in Fig. 2 is demonstrated in Fig. B1 and the related transfer function is derived as:

$$\frac{V_{out}(s)}{V_{RF}(s)} = \frac{g_m L_{p2} L_1 S^2}{L_{p2} L_1 C_{p1} C_{p2} S^4 + L_{p2} L_1 C_{p2} S^3 + (L_1 C_{p1} + L_{p2} C_{p2}) S^2 + L_1 S + 1} \quad (B1)$$

where $L_{p2} = L_{2N} \parallel L_2$, $C_{p1} = C_{gs} + C_1 + (C_{gd} + C_f) \cdot A_{v0}$, $C_{p2} = C_N + C_2$. As can be seen in the expressions, the second oscillator's inductance and capacitance are affected by the nonlinearity effects as L_{2N} and C_N and the first oscillator is just influenced by the gain of the circuit $A_{v0} \sim g_m r_0$, where r_0 is the resistance generated due to the channel length modulated effect. The step response of the transfer function expressed in Eq. B1 is illustrated in Fig. B2. It is shown that the settling time is around 80 nsec; this time is very close to t_0 that we selected based on the oscillators decay rates. In fact, t_0 is selected around the settling time for the system.

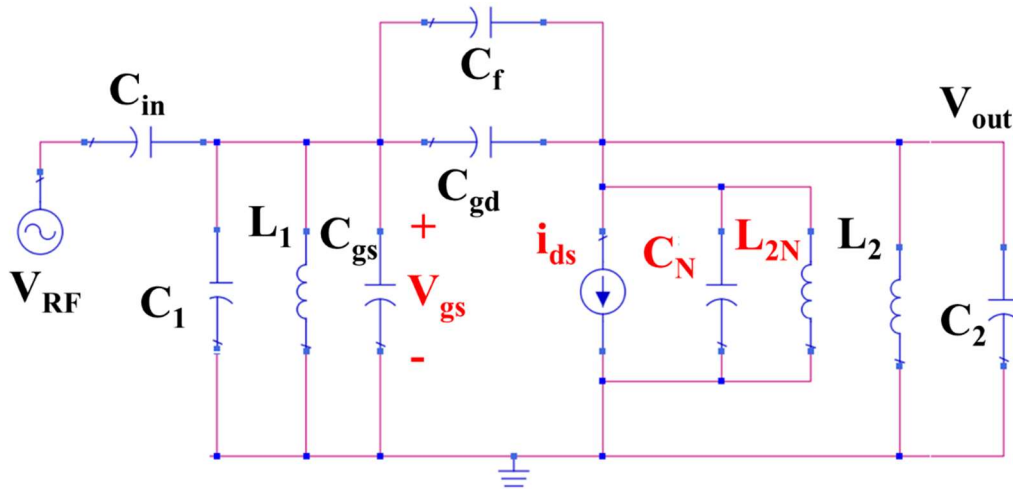


Fig. B1 A simplified version of the circuit to estimate about the transfer function.

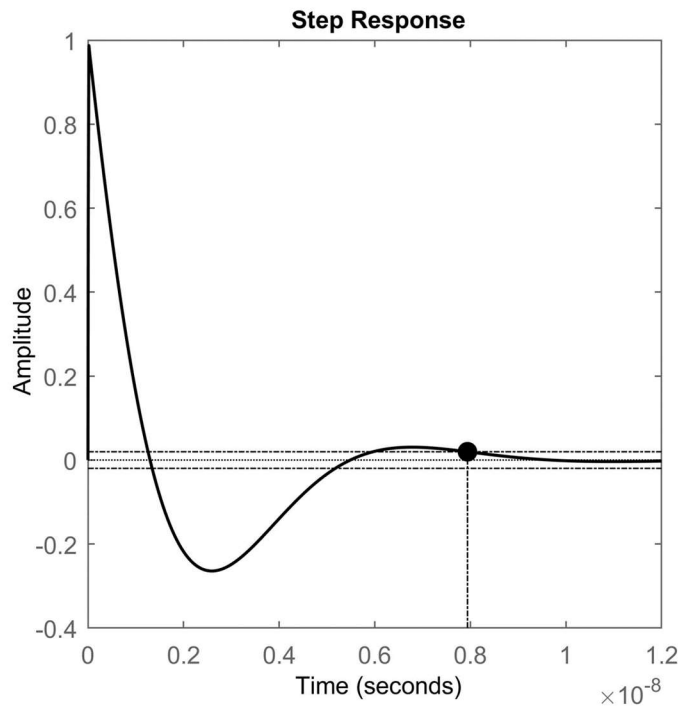


Fig. B2 Step response of the circuit.